The Japan Society of Mechanical Engineers

Effects of Gas Inertia Forces on Dynamic Characteristics of Externally Pressurized Gas-Lubricated Thrust Bearings*
(Bearing Performance of Externally Pressurized Gas-Lubricated Circular Thrust Bearings with a Single Central Supply Hole in a Choked Condition)

Yoshio HARUYAMA**, Atsunobu MORI***,
Haruo MORI***, Fusao MIKAMI**,
Tsuneji KAZAMAKI**** and Hiroki AIKAWA†

In this paper, two analytical models for an externally pressurized circular thrust bearing with a central supply hole are presented when the gas flow is choked at the inlet to the clearance space. These models can be modified for an unchoked condition and enable one to analyze the dynamic performance of the bearing over a wide range of design conditions. From the experiment, it is concluded that the effects of the inertia forces are considerable when the feeding parameter is small, and that the presented analyses yield good predictions of both the bearing stiffness and the damping coefficient.

Key Words: Lubrication, Theoretical Analysis, Externally Pressurized Gas Bearing, Inertia Effect, Dynamic Performance, Choked Flow

1. Introduction

Conventional analyses of the performance of externally pressurized gas-lubricated bearings are based on the classical Reynolds equation in which the inertia forces of the gas film are ignored and an isothermal change of state of the gas film is assumed. Several investigators have found the effects of the inertia forces on the static and dynamic performance to be small for usual applicationos[(1)~(3)]. Some of the authors have already pointed out the fact that the inertia forces of the gas film cannot be ignored in the analysis of the damping coefficient when the Reynolds number of the pressure flow becomes high[(4)]. In the present paper, the dynamic characteristics of externally pressurized circular thrust gas bearings with a single central supply hole will be investigated. In such a bearing, a sharp depression in the pressure profile near the supply hole has been observed for the case of high supply-pressure and large clearance. Mori and coworkers[(5)~(9)] investigated theoretically and experimentally the above problem and presented that the pseudo shock wave model yielded good predictions for the statical pressure profile. It is difficult, however, to analyze the dynamic performance by this model. In this paper, therefore, new simplified models are introduced to enable the determination of the dynamic performance of such a bearing. In these new models, it is assumed that the complicated flow in the region of the static pressure recovery just after supersonic expansion around the feed hole can be replaced by an inertia-dominated isothermal flow. Such an isothermal inertial flow is followed by an isothermal fully developed flow. This fully developed flow is analyzed through the Navier-Stokes equations by means of the averaging approach[(4)]. Such models enable the determination of the statical pressure profile similar to that obtained by using the pseudo-shock-wave model which coincides well with the experimental profile.

* Received 21 th October, 1987. Paper No. 86-1155 A
** Faculty of Engineering, Toyama University, 3190 Gofuku, Toyama, 930, Japan
*** Faculty of Engineering, Kyoto University, Yoshida Hon-Machi, Sakyo-ku, Kyoto, 606, Japan
**** 1740-1908 Hirai Aza Minamitanishita, Kan-nami-cho, Tagata-gun, Shizuoka, 419-01, Japan
† Nippon Mektron Co., Ltd., 1-12-15 Shiba-Daimon, Minato-ku, Tokyo, 105, Japan

NII-Electronic Library Service

The Japan Society of Mechanical Engineers

2. Theoretical Analysis

Figure 1 shows schematically the externally pressurized circular thrust gas bearing with a single central supply hole of inherent compensation which is subjected to analysis. This bearing has a uniform film thickness without any recess. The gas with constant pressure p_s is fed into a central hole. It is presupposed that the gas behaves as the perfect gas, and that the flow is choked at the inlet to the clearance space. The following assumptions are used in order to simplify the analysis.

1) As shown in Fig. 1, the flow domain in the clearance space can be divided into three regions, namely, Region I with a supersonic isentropic flow, Region II with an inertia-dominated isothermal flow and Region III with a subsonic fully developed flow.

2) The flow in Region I is, as mentioned above, isentropic, and the skin friction is negligible. The heat transfer from the walls is also negligible. Dynamical conditions can be analyzed quasi-statically. Velocity profile across the film thickness is always uniform.

3) The flow in Region II is inertia-dominated and isothermal. Viscous effect on the velocity profile is negligible. Dynamical conditions can be analyzed quasi-statically.Velocity profile across the film thickness is always uniform.

4) The flow in Region III is fully developed, laminar and isothermal. Inertia forces are taken into account. Dynamical conditions can be analyzed through the unsteady Navier-Stokes equations by means of the averaging approach.

The boundary conditions are the continuity of the pressure and the mass rate of flow at the boundaries between adjacent regions. It is assumed that the maximum statical velocity in Region III is equal to the sonic velocity at the beginning of Region III.

(i) Region I : The momentum equation, continuity equation, equation of state and energy equation are given as follows :

$$-\frac{1}{\rho}\frac{dp}{dr}=u\frac{du}{dr} \tag{1}$$

$$\frac{d}{dr}(r\rho u)=0 \tag{2}$$

$$p\rho^{-1}=\mathcal{R}\,T \tag{3}$$

$$C_p dT+d(u^2/2)=0 \tag{4}$$

where u is the velocity component in the r-direction, p is the pressure, ρ the density, $\mathcal{R}$ the gas constant, T the absolute temperature and C_p the specific heat at constant pressure.

The gas enters Region I with sonic velocity and critical pressure p^* corresponding to the supply pressure p_s. p^* is written by

$$p=p^*=\left(\frac{2}{\varkappa+1}\right)^{\varkappa/(\varkappa-1)}\cdot p_s. \tag{5}$$

From Eqs.(1) to (4), the pressure in Region I is obtained as

$$\left(\frac{R_s}{R}\right)^2=\frac{\varkappa+1}{\varkappa-1}\left(\frac{P}{P^*}\right)^{2/\varkappa}-\frac{2}{\varkappa-1}\left(\frac{P}{P^*}\right)^{(\varkappa+1)/\varkappa} \tag{6}$$

where $P=p/p_a$, $P^*=p^*/p_a$, $R=r/r_0$, $R_s=r_s/r_0$ and $\varkappa$ is the ratio of specific heats.

(ii) Region II : The momentum equation and the continuity equation are the same ones as in Region I . The equation of state is given by

$$p\rho^{-1}=\mathcal{R}\,T_0 \tag{7}$$

where T_0 is the ambient absolute temperature which is constant. From these equations, the following equation can be obtained

$$\frac{dP}{dR}=\frac{P}{R}\frac{C_{II}^2}{P^2R^2-C_{II}^2} \tag{8}$$

where C_{II} is the integration constant. In order to calculate numerically as easily as possible, Eq.(8) is transformed approximately as follows ;

$$\frac{dP}{dR}=\frac{C_{II}^2}{PR^3}\left(1+\frac{C_{II}^2}{P^2R^2}\right) \tag{9}$$

or

$$\frac{dP}{dR}=\frac{C_{II}^2}{PR^3} \tag{10}$$

since $C_{II}^2/(P^2R^2)<1$ in Region II (refer to Appendix 1).

The result derived from Eq.(9) is named Solution 1 and that from Eq.(10) is named Solution 2 in the following discussion. Equation(10) can be solved analytically as

$$P=\left(-\frac{C_{II}^2}{R^2}+C'_{II}\right)^{1/2} \tag{11}$$

where C'_{II} is the integration constant.

(iii) Region III : The momentum equations, continuity equation and equation of state are given as follows ;

$$\rho\left(\frac{\partial u}{\partial t}+u\frac{\partial u}{\partial r}+w\frac{\partial u}{\partial z}\right)=-\frac{\partial p}{\partial r}+\mu\frac{\partial^2 u}{\partial z^2} \tag{12}$$

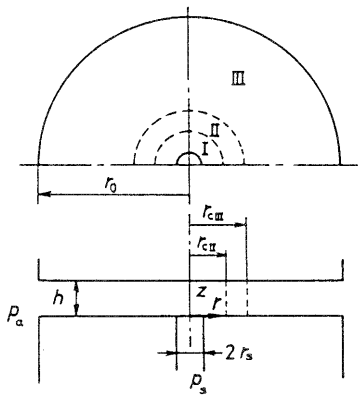

Fig. 1 Schematic diagram of externally pressurized thrust bearing

NII-Electronic Library Service

The Japan Society of Mechanical Engineers

$$0=\frac{\partial p}{\partial z} \tag{13}$$

$$\frac{\partial \rho}{\partial t}+\frac{1}{r}\frac{\partial}{\partial r}(r\rho u)+\frac{\partial}{\partial z}(\rho w)=0 \tag{14}$$

$$p\rho^{-1}=\mathcal{R}\,T_0 \tag{15}$$

where w is the velocity component in the z-direction, t is the time and μ the viscosity. It is quite difficult to obtain the solutions for the above equations without any approximations. Then, averaging out all the inertia terms in the momentum equation (12) across the film thickness, and defining f as

$$f\equiv\frac{1}{\mu}\frac{\partial p}{\partial r}+\frac{\rho}{\mu h}\int_0^h\left(\frac{\partial u}{\partial t}+u\frac{\partial u}{\partial r}+w\frac{\partial u}{\partial z}\right)dz \tag{16}$$

we can obtain the following pressure equations;

$$\frac{H^3}{R}\frac{\partial}{\partial R}(RPF)=\sigma\frac{\partial}{\partial \tau}(PH) \tag{17}$$

$$F=\frac{\partial P}{\partial R}+1.2a\frac{H^4}{R}\frac{\partial}{\partial R}(RPF^2)-\frac{a\sigma}{H}\frac{\partial}{\partial R}(PFH^3) \tag{18}$$

where

$$H=h/h_0,\ \tau=\omega t,\ F=r_0\mu f/p_a,$$

$$\sigma=\frac{12\mu\omega}{p_a}\left(\frac{r_0}{h_0}\right)^2,\ a=\left(\frac{p_a h_0^2}{12\mu\sqrt{\mathcal{R}\,T_0}\,r_0}\right)^2$$

h_0 is the equilibrium clearance, p_a the ambient pressure, and ω the angular frequency of squeeze motion. a is a parameter which represents the contribution from the inertia forces[4], and σ is the squeeze number. The velocity profile across the film thickness is always obtained as a parabolic shape.

Now suppose a small harmonic variation around the equilibrium state. Then, the clearance H can be given by

$$H=1+\varepsilon e^{j\tau}. \tag{19}$$

Corresponding to this, P and F are given by

$$(P,\ F)=(P_0,\ F_0)+\varepsilon(\hat{P}_t,\ \hat{F}_t)e^{j\tau} \tag{20}$$

Substituting Eqs.(19) and (20) into Eqs.(17) and (18), we can formulate the following governing differential equations;

$$\frac{dP_0}{dR}=\frac{P_0}{R}\frac{C_{\mathrm{III}}R^2+1.2aC_{\mathrm{III}}^2}{P_0^2R^2-1.2aC_{\mathrm{III}}^2} \tag{21}$$

$$\frac{1}{R}\frac{d}{dR}\{R(P_0\hat{F}_t+\hat{P}_tF_0)\}=j\sigma(P_0+\hat{P}_t) \tag{22}$$

$$\hat{F}_t=\frac{d\hat{P}_t}{dR}+\frac{1.2a}{R}\frac{d}{dR}\times\{R(4P_0F_0^2+2P_0F_0\hat{F}_t+\hat{P}_tF_0^2)\}-ja\sigma\{P_0(\hat{F}_t+3F_0)+\hat{P}_tF_0\} \tag{23}$$

where C_{III} is the integration constant. In order to calculate numerically as easily as possible, Eq.(21) is transformed approximately as follows;

$$\frac{dP_0}{dR}=\frac{1}{P_0R^3}(C_{\mathrm{III}}R^2+1.2aC_{\mathrm{III}}^2)\left(1+\frac{1.2aC_{\mathrm{III}}^2}{P_0^2R^2}\right) \tag{24}$$

or

$$\frac{dP_0}{dR}=\frac{C_{\mathrm{III}}R^2+1.2aC_{\mathrm{III}}^2}{P_0R^3} \tag{25}$$

since $1.2aC_{\mathrm{III}}^2/(P_0^2R^2)<1$ in Region III (refer to Appendix 2).

Equation(24) is used in Solution 1 corresponding to Eq.(9), and Eq.(25) is used in Solution 2 corresponding to Eq.(10). Equation(25) can be solved analytically as

$$P_0=\left\{2C_{\mathrm{III}}\ln R-1.2aC_{\mathrm{III}}^2\left(\frac{1}{R^2}-1\right)+1\right\}^{1/2}. \tag{26}$$

Equations(9),(24),(22) and (23) are calculated numerically by the Runge-Kutta-Gill method.

The dynamic stiffness and the damping coefficient are defined as the component of the bearing reaction force in the same phase as the displacement, and the component in the same phase as the velocity of the displacement, respectively. The dimensionless dynamic stiffness K and the dimensionless damping coefficient B normalized respectively by $\pi r_0^2p_a/h_0$ and $\pi r_0^2p_a/(h_0\omega)$ can be derived using the four dimensionless designing parameters: $R_s=r_s/r_a$ (the dimensionless radius of the supply hole), $P_s=p_s/p_a$ (the dimensionless supply pressure), $\Gamma=-12\mu C_Dr_s\sqrt{\mathcal{R}\,T_0}\ln R_s/(p_ah_0^2)$ (the feeding parameter) and $R_e^{**}=\rho_0h_0^2\omega/\mu$ (the unsteadiness parameter), and the discharge coefficient C_D. ρ_0 is the density at the ambient pressure p_a. R_e^{**} is equivalent to the Reynolds number obtained using the velocity of the squeeze motion $h_0\omega$ as the characteristic velocity. This parameter represents the ratio of the local acceleration term to the viscous term. The above parameters are related to the squeeze number σ and the inertia parameter a defined in Eqs.(17) and (18) by the following equations;

$$\sigma=\frac{1}{12}\left(\frac{-\Gamma}{C_DR_s\ln R_s}\right)^2Re^{**} \tag{27}$$

$$a=\left(-\frac{C_DR_s\ln R_s}{\Gamma}\right)^2. \tag{28}$$

The analytical models in this paper can be modified for an unchoked condition. In this case, Region I disappears and the bearing clearance space is divided into two regions, Region II and Region III. If the value of Γ becomes large, the whole space can be treated as Region III only.

3. Examples of Calculated Results

To verify the basis of the proposed analysis, in Fig. 2, the theoretical estimations of the statical pressure profile are compared with the experimental results[13]. In this figure, the symbols, PM and LT indicate the results by the 1st-order perturbation method[10] and the classical lubrication theory, respectively. The results of ref.(8) are obtained by using the pseudo-shock-wave model. $R_{c\mathrm{II}}$ and $R_{c\mathrm{III}}$ are the radial positions of the termination of Regions I and II obtained by Solution 1. The radial position, $R_{c\mathrm{II}}$, of the termination of the supersonic isentropic flow region calculated by Solution 1 or Solution 2 is located far upstream from the corresponding position calculated

NII-Electronic Library Service

The Japan Society of Mechanical Engineers

by the pseudo-shock-wave model. The theoretical results agree well with the experimental data.

Figure 3 shows the results of the various approximate solutions for the dynamic stiffness and the damping coefficient. In this figure, the symbol AA indicates the results by the averaging approach[4]. There is no significant difference between Solution 1 and Solution 2. As for K and B, under the condition where Γ is small, the results of Solutions 1 and 2 are larger than those of LT. The results of AA are nearly equal to those of Solutions 1 and 2. However, the results of AA cannot be, obtained under the condition where the gas flow is choked at the inlet to the clearance space. The inertia effects by PM are smaller than those by Solutions 1 and 2.

Figures 4 and 5 show the influence of R_s and p_s on K and B. In these figures, the solid lines correspond to Solution 1 and the broken lines to the classical lubrica-

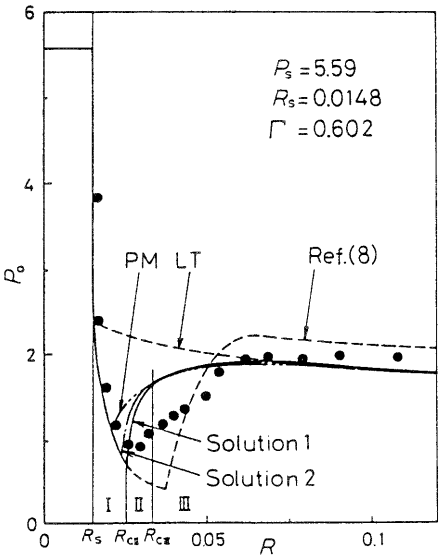

Fig. 2 Comparison with experiment[13], for statical pressure profile

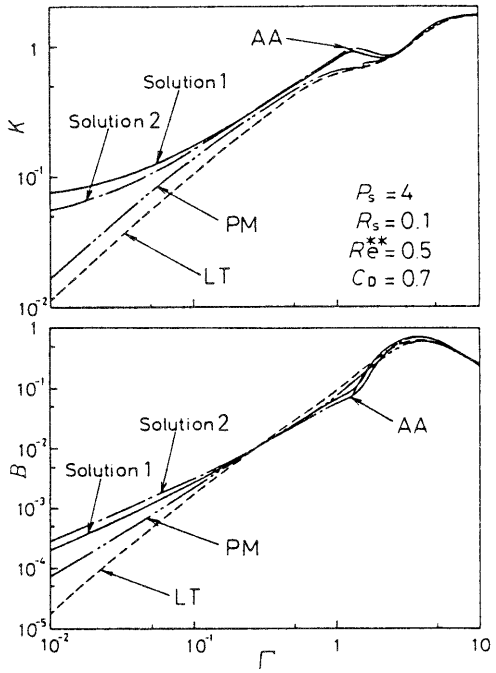

Fig. 3 Comparison of approximate solutions for dynamic stiffness and damping coefficient

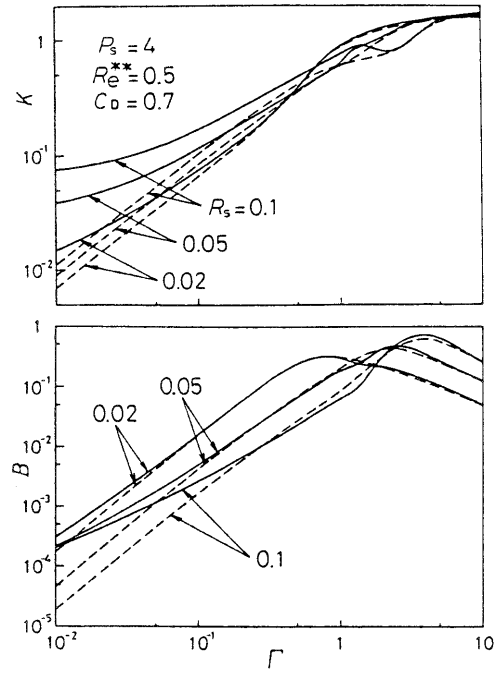

Fig. 4 Dynamic stiffness and damping coefficient for different radii of supply hole R_s

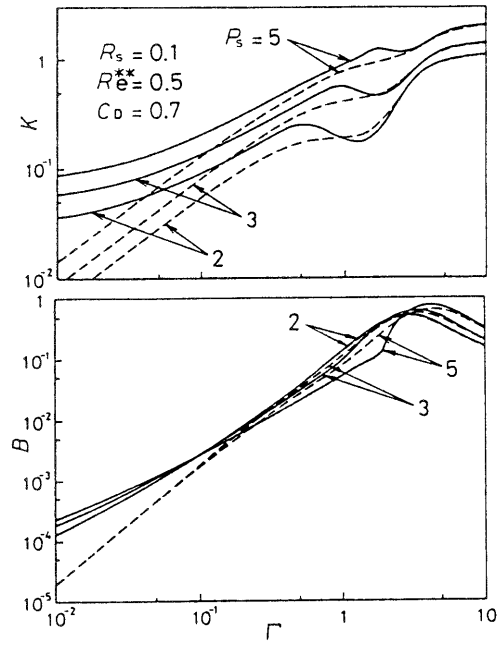

Fig. 5 Dynamic stiffness and damping coefficient for different supply pressures P_s

NII-Electronic Library Service

The Japan Society of Mechanical Engineers

tion theory. The inertia effects become remarkable as the radius of the supply hole R_s increases. However, the effects are almost the same in magnitude even if the supply pressure p_s increases.

4. Comparison with Experimental Results

The experimental apparatus and procedure are the same as reported in Ref.[11]. The bearing stiffness and the damping coefficient are obtained by the following method. An impulse load is applied to the shaft. The response of the shaft displacement is recorded by a digital memory and displayed on an oscilloscope. The logarithmic decrement and frequency of shaft vibration are determined from these data, and are then used to calculate the stiffness and the damping coefficient. The mass of shaft is 1.50 kg. The dimensions of the test bearing are $2r_0=45$ mm and $2r_s=5$ mm.

In Figs. 6 and 7, the calculated results of K and B are compared with the experimental results. In Fig. 6, the influence of P_s is examined. The solid lines and the broken lines indicate the results of Solution 1 and the classical lubrication theory, respectively. In this figure, good agreement can be found between the estimations by the present theory and the experimental data. This is pronounced under high supply-pressure conditions. In Fig. 7, the theoretical results obtained by using the various analytical models are compared with the experimental data in the case of $P_s=3$. This figure has the same symbols as Fig. 3. In both K and B, the predictions by Solutions 1 and 2 are very close to the experimental data, while those by PM and LT tend to be much lower than the experimental data. This is pronounced as h_0 increases. Availability of AA is limited within a relatively small clearance.

The value of the discharge coefficient C_D is determined by using the contraction ratio for a sharp-edged orifice presented in Ref.[12].

5. Conclusions

New analytical models are introduced to predict the effects of the inertia forces of a gas film flow on the dynamic properties of an externally pressurized gas-lubricated circular thrust bearing with a single central supply hole. From comparison with the experiment, the following conclusions have been obtained:

(1) The new model enables the analysis of the dynamic performance of such a bearing over a wide range of design conditions. The calculated results of the dynamic stiffness and damping coefficient agree well with the experimental data.

(2) There is no significant difference between Solutions 1 and 2 of the model. It can be concluded that Solution 2, which is more simplified, is better for

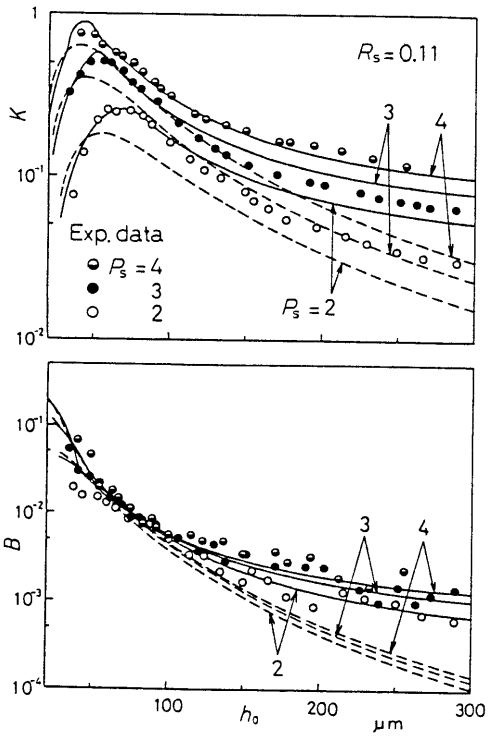

Fig. 6 Results of Solution 1 and the classical lubrication theory compared with experiment, for dynamic stiffness and damping coefficient

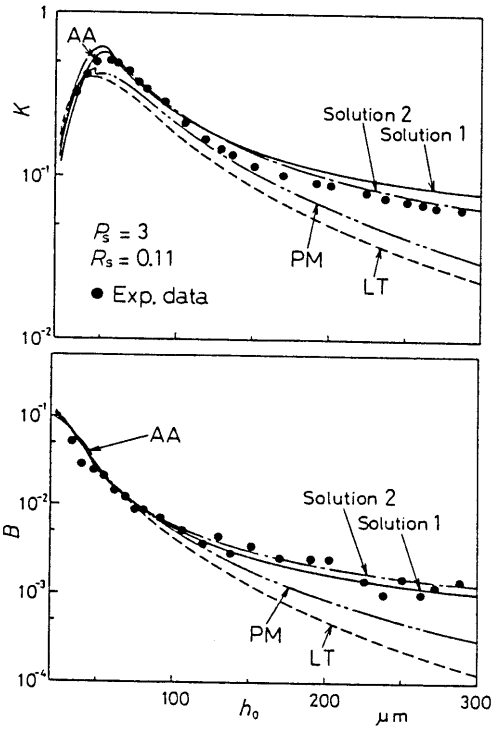

Fig. 7 Results of various analytical models compared with experiment, for dynamic stiffness and damping coefficient

NII-Electronic Library Service

The Japan Society of Mechanical Engineers

practical use because the statical pressure profile in it can be obtained analytically.

(3) The inertia effects become remarkable as the radius of the supply hole R_s increases, however, the effects are almost independent of the supply pressure P_s.

(4) The inertia effects predicted by the perturbation method are, in general, much smaller than the experimental results.

Acknowledgment

The authors would like to thank Mr. T. Sakurai, student of the Faculty of Engineering of Toyama University, for his assistance in the present work.

Appendix 1

Integrating the continuity equation, the following equation is obtained;

$$RPU = C_{II} \tag{29}$$

where $U = u/\sqrt{\mathcal{R}\,T_0}$. Therefore, $C_{II}^2/(P^2R^2)$ is given by

$$C_{II}^2/(P^2R^2) = U^2. \tag{30}$$

The velocity profile across the film thickness in Region III is parabolic and the maximum statical velocity is assumed equal to the sonic velocity $\sqrt{x\mathcal{R}\,T_0}$ at the boundary $r = r_{cIII}$ between Region II and Region III. The velocity profile in Region II is uniform. Therefore, the velocity in Region II at the boundary $r = r_{cIII}$ is equal to $2\sqrt{x\mathcal{R}\,T_0}/3$ in order to conserve the mass flow rate. Thence, $U|_{R=Rc_{III}} = 2\sqrt{x}/3$. The value of U increases as R decreases. Since dP/dR has finite values, the following expression is derived in Region II:

$$\frac{4x}{9} \leqq \frac{C_{II}^2}{P^2R^2} < 1. \tag{31}$$

Appendix 2

From Eqs.(12) and (16), the following equation is obtained:

$$\frac{\partial^2 u}{\partial z^2} = f. \tag{32}$$

The nondimensional statical components are written as

$$F_0 = \frac{1}{12\sqrt{a}} \frac{\partial^2 U_0}{\partial Z^2}. \tag{33}$$

On the other hand, from Eqs.(17) to (20), the following equation is obtained:

$$\frac{d}{dR}(RP_0F_0) = 0. \tag{34}$$

Integrating this equation, we get

$$F_0 = C_{III}/(RP_0). \tag{35}$$

From Eqs.(33) to (35), the following equation is obtained

$$\frac{1.2aC_{III}^2}{P_0^2R^2} = \frac{1}{120}\left(\frac{\partial^2 U_0}{\partial Z^2}\right)^2. \tag{36}$$

Since the profile for U_0 is parabolic, the following equation can be obtained:

$$1.2aC_{III}^2/(P_0^2R^2) = 8U_{max}^2/15 \tag{37}$$

where $U_{max} = U_0|_{z=1/2}$. U_{max} has the maximum value $\sqrt{x}$ at the boundary between Region III and Region II. Thence, the following expression is derived in Region III:

$$0 < \frac{1.2aC_{III}^2}{P_0^2R^2} \leqq \frac{8x}{15} \tag{38}$$

When the lubricant is air, $x = 1.4$, so $0 < 1.2aC_{III}^2/(P_0^2R^2) < 0.747$.

References

(1) Gross, W. A., Gas Film Lubrication, (1962), p. 255, John Wiley & Sons.

(2) Sato, K. and Mori, H., Trans. Jpn. Soc. Mech. Eng., (in Japanese), Vol. 41, No. 347 (1975), p. 2189.

(3) Sato, K., Kyoto Univ., Doctor's Thesis, (in Japanese), (1976), p. 33.

(4) Mori, A., Iwamoto, N. and Mori, H., Bull. JSME, Vol. 22, No. 173 (1979), p. 1678.

(5) Mori, H., Trans. Jpn. Soc. Mech. Eng., (in Japanese), Vol. 26, No. 169 (1960), p. 1249.

(6) Mori, H., Miyamatsu, Y. and Sakata, S., J. Jpn. Soc. Lubr. Eng., (in Japanese), Vol. 9, No. 2 (1964), p. 113.

(7) Mori, H. and Miyamatsu, Y., J. Jpn. Soc. Lubr. Eng., (in Japanese), Vol. 11, No. 11 (1966), p. 457.

(8) Mori, H. and Ezuka, H., Prepr. JSLE-ASLE Int. Lubrication Conf. of (1975), p. 115.

(9) Mori, H. and Sakata, S., J. Jpn. Soc. Lubr. Eng., (in Japanese), Vol. 10, No. 5 (1965), p. 435.

(10) Haruyama, Y., Mori, A., Kazamaki, T. Mori, H. and Nakamura, T., Trans. Jpn. Soc. Mech. Eng., (in Japanese), Vol. 51, No. 471, C (1985), p. 2877.

(11) Haruyama, Y. and Mori, H., Bull. JSME, Vol. 25, No. 210 (1982), p. 2030.

(12) Shapiro, A. H., The Dynamics and Thermodynamics of Compressible Fluid Flow, (1953), p. 358, The Ronald Press Co..

(13) McCabe, J. T., Elrod, H. G., Carfagns, S. P. and Colsher, R., Franklin Inst. Res. Lab. Interim Rep., I-C-2429-1 (1969).

NII-Electronic Library Service